

Orientation Detection of Unequally Spaced Complexed Grounding Grids using Transient Electromagnetic Method

Usman Zia Saleem¹, Safdar Raza¹, Inzamam Ul Haq², Muhammad Bilal Ashraf¹

Abstract:

Configuration of Grounding Grid is required for all currently proposed Fault Diagnosing methods of Grounding Grid if the configuration is unknown then Grounding Grid Configuration detection techniques are applied and all of these latest techniques further requires the oriented angle at which the grid is laid and if the orientation of the grid is unknown or incorrect then the calculated configuration will be misleading and incorrect and we will fail to diagnose the Grounding Grid Fault. In this paper Transient Electromagnetic Method approach is used for orientation detection of Unequally Spaced Grounding Grids which are categorized as complexed grids further classified as Unequally spaced grounding grids with diagonal element at larger mesh, smaller mesh or in both of these meshes. In TEM method Equivalent Resistivities and Magnetic Field Intensities are found at eight different points in a circular path of constant radius r to determine the size of meshes and the presence of conductors whether diagonal or not diagonal. Model Designing and Simulations are performed using COMSOL Multiphysics 5.4 software, values of Magnetic Field Intensities and EMF are derived from COMSOL Multiphysics 5.4 software and the EMF values are further called in a MATLAB code to run through number of mathematical formulations and Equivalent Resistivity is obtained for all desired points. Obtained values of Equivalent Resistivity and Magnetic Field Intensities verifies the effectiveness of the proposed approach for orientation detection of complexed grounding grid.

Keywords: *Equivalent Resistivity, Grounding Grid, Magnetic Field Intensity, Orientation Detection, Transient Electromagnetic Method*

1. Introduction

Grounding system provides alternate route to the high flowing currents due to any risk of Fault by sinking high currents through Earth before the Fault gets worst in form of electrical shock or hazardous fire. Grounding means low resistive path between any desired electrical equipment and the ground. Grounding is achieved by properly connecting the electrical equipment through cable into the ground using

relatively large extent of body to maximize the contact area with earth and keep the potential of connecting body to the potential of Ground [1]. The depth of the grounding system depends upon the value of resistance it offers NEC recommends that if the grounding rods are to be considers for grounding than 8 to 10 foot ground rod fails to meet the minimum resistance requirement Mostly 30 foot provides us with 5 ohm or less resistance

¹ Department of Electrical Engineering, NFC Institute of Engineering & Technology, Multan, Punjab, Pakistan

² State Key Laboratory of Power Transmission Equipment & System Security and New Technology, Chongqing University, Chongqing 400044, China

Corresponding Author: safdar.raza@nfciet.edu.pk

which is feasible and the grounding resistance changes mostly in the first 20 foot.

In a substation the grounding system consists of horizontally placed interlinked bare conductors with equal or unequal spacing within few meters apart, buried below the earth surface at about 0.7 to 1 meter depth.

Grounding system as discussed above provide finite resistance 1 ohm for Large Stations 1-5 ohm for distribution substations relatively small. This resistance is known as Ground resistance. The Potential of the Grounding system is zero under normal conditions. Under faulty condition when large amount passes into the earth then the Ground potential of the faulty area rises with respect to the Ground potential of remote earth away from the faulty area. So the potential rise of the specified part of the earth is known as GPR ground potential rise and it value increases with the severity of the fault and the increase in faulty current.

Mesh Voltage and Step Voltage are two essential parameters which depends upon the value of Ground resistance and GPR. The conductors present in the grounding grid system divide these voltages into the meshes present under the surface and the potential on the earth surface. Mesh voltage is the maximum value of touch voltage offered within a specified surrounding. Step Voltage is the potential difference between the feet of a

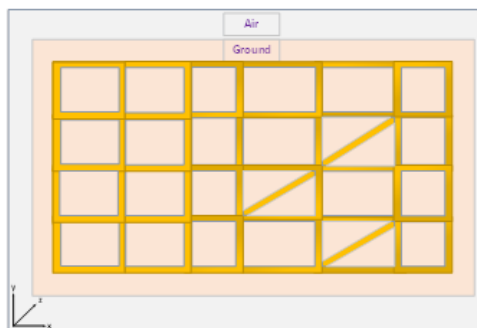


Fig. 1. Unequally Spaced Grounding Grid with diagonal conductors.

person standing near an energized grounding grid when the fault is occurring.

Human Body offers non inductive impedance and purely resistive impedance for DC/AC voltage of 50 or 60 Hz standard implemented worldwide. Human body offers resistance from 500 to 5000 ohm but the average value is mostly considered as 1000 ohm [2].

The Low impedance path is provided by installing Grounding Grid and can be found on all stages of Electrical network from Power Plants to Distribution units known as substations. The Grounding grid is made of Steel, Cooper clad wires, Galvanized steel and Cooper Steel Alloys. These conductors are joint together and buried under the soil switched for Lightning Strokes and Surges produced while switching high power loads [3, 4].

Grounding Grid's efficiency depends upon the condition of conductors of Grounding Grid the conductors can be damaged due to corrosion due to presence of air gaps consisting Oxygen and the moisture. Both these elements begin the process of oxidation of conductors and damages the conductor current carrying capacity and can lead on to cut off the path entirely through Breakdown of conductors. Life estimation of Grounding grid depends upon the overall size of Grounding Grid and also the precautionary preventive maintenances done over the regular recommended intervals [5] Performance can be enhanced by reducing fault currents [6] or optimizing the overall configuration of Grounding Grid [7].

High Faults currents in Grounding Grid can result in thermal and mechanical stresses so in case if we are unable to reduce the fault then we are required to design Grounding Grid to bear the offered high faulty current [8].

2. Related Work

Transient analysis technique is quite old and have been using for grounding systems using different models such as Transmission Line models (TL Models) [9-13]. Circuit Theory Models [14, 15] and Antenna theory models [16-21]. Researches are also performed on Comparative analysis between

Transmission Line Models and Antenna Theory Models [20, 22].

Circuit Theory Model is quite old and significantly simplified model due to which its accuracy is compromised also, we need to mention that surge propagation delay cannot be predicted using circuit theory model. TL Transmission Line method is feasible for finding surge propagation delay and computational cost of this transient analysis technique is less but TL method does not consider earth-air interface so ultimately the solution is compromised for some higher frequencies. Antenna theory models are best for small grounding grid system as it the most accurate with high computational time and the complexity of this technique increases with the size of grounding grid.

Previously research work have been performed on finding Grounding Grid Orientation through TEM method but only for Equally Spaced and Unequally Spaced without diagonal and the recommended more work needs to be done for Unequally spaced Grounding Grids with Diagonal Branches and this paper covers all the recommended research scopes [23].

a) FAULT DIAGNOSIS

There are multiple research groups which are currently working on fault diagnosis of grounding grid. These research fields are mentioned below.

- i. Electric Network Theory Method.
- ii. Electromagnetic Field Theory Method.
- iii. Electrochemical Detection Theory Method.

In Electric Network Theory Method we form nonlinear equations using surface potential difference and port resistance [24-28] these nonlinear equations can further used to diagnose grounding grid faults easily but this method requires the data regarding configuration of grounding grids.

Electrochemical Methods can easily identify the corrosion of grounding grid

conductors but the cannot find the breakage point of grounding grid [29].

Transient Electromagnetic method [30-32] is most feasible so far in this method ramp shaped current signal is injected he change in magnetic field produces secondary currents in the grounding conductor present below the ground level through which equivalent resistivity is calculated using inversion calculations these values of resistivity are used to identify faults in grounding grid.

b) CONFIGURATION

Configuration of grounding grid can be used as fault detection and also for improving the efficiency of the Grounding Grid. Research group working on the relation between the efficiency and the changing configuration but the research group related to the configuration for fault diagnosis is not so active and creates a research gap [33]. First method is to record the magnetic intensity produced on the surface of the earth created due to the injection of sinusoidal current in the grounding mesh [34]. Derivative Methods are also quite famous for finding topology by applying 1st and 3rd derivatives on the magnetic field intensity recorded on the surface of the grid [35]. For specified angled branches the configuration can be found by taking circle and line derivatives of the magnetic flux density found on the surface of the earth [36]. Transient Electromagnetic Method is the latest and most accurate method for finding the configuration of the Grounding grid.

c) ORIENTATION

As we have already discussed that fault diagnosis is done accurately when the configuration of the grid is known but the configuration of the grounding grid is not always known and configuration of old grounding grids which have most probability of getting faulty are mostly unknown or lost so here the configuration detection techniques are applied all of the so far known techniques delivers inaccurate results if the grounding grid is installed at an angle to the plane of earth as we usually consider it parallel to the plane of earth for finding configuration so when the detected configuration is not accurate we will

be unable to trace the faults in grounding grid as we may have gone on a wrong track initially ultimately getting nowhere near the fault so from the above discussion we can verify that accurate configuration of the Grounding Grid and the accurate location of faults can be diagnosed if we have the knowledge about at what angle the grid is laid.

So far there is proposed method for orientation detection of grounding grid derivative method based novel techniques along with the concept of finding geometry of mesh to further find out the angle of the grounding grid [37]. In this method direct current is injected in to the grounding grid mesh and as a result the magnetic field density are recorded on the surface of the earth derivatives are take of these densities in a circular path starting from the center of a vertical conductor so all the adjacent branches are found in 360 degrees.

The main drawback of the above-mentioned technique is that noise may add in the generated magnetic fields densities of the grounding grid by interacting with the external Electromagnetic fields of the nearby equipment.

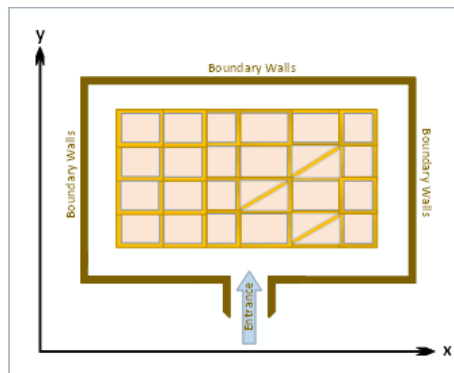


Fig. 2. Grounding Grid installed parallel to the Station.

As we have discussed earlier the importance of the orientation detection of Grounding Grid. I propose a TEM method for orientation detection of grounding grid so that we don't have to waste time on soil excavation

of entire grid despite a specified point where fault exists.

When we manage to find the Oriented angle of the grid we can then proceed further to detect its complete configuration or Topology which was previously not known due to the mishandling if the Diagrams or not following Diagram while erection of grounding grid or changing the angle parameters last minute to overcome any physical challenge faced a that time.

So, this Methodology comes in handy whenever the angle of the grid is unknown or varies from the mentioned angle provided in manuals whenever the grid is not parallel to the earth's plane.

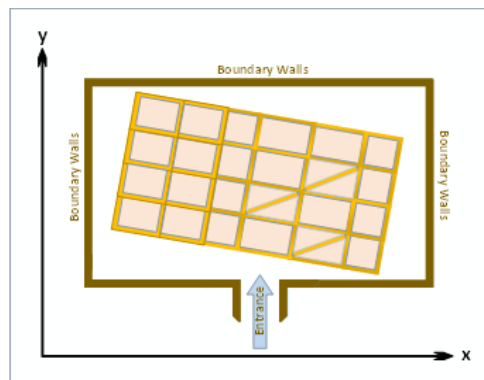


Fig. 3. Grounding Grid installed at an angle to the Station.

3. Proposed Methodology

3.1. Transient Electromagnetic Method TEM

TEM is mostly popular for Geological Exploration for Onshore exploration and Offshore exploration. Exploration of Minerals, Oil, Gas and Ground Water is performed and also being used for environmental mapping. Water filled mining, Tunnel designing [38-44].

The Figure 4 is the schematic layout of a Basic TEM system which consists of two coils one of them is transmitter coil and one of them is receiver coil. Transmitter coil also known as primary coil is injected with current pulse of ramp wave as a result magnetic field is produced when current ramp signal is switched

off as a result during switching time an emf is produced in the surrounding conductor this stored emf further produced secondary magnetic field in the transmitter coil while the current signal is still switched off.

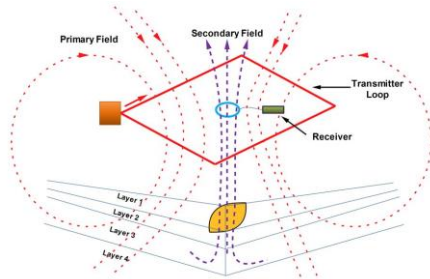


Fig 4. Diagram of Generalized Transient Electro Magnetic Method.

The Figure 5 shows the injected ramp current wave which has both ON time and OFF time ramp signal are used to switch ON and switch OFF the current during switching OFF time period due to changing value of decreasing current EMF is induced in the opposite direction this EMF is further discharged in form of Magnetic Field during OFF time of current signal.

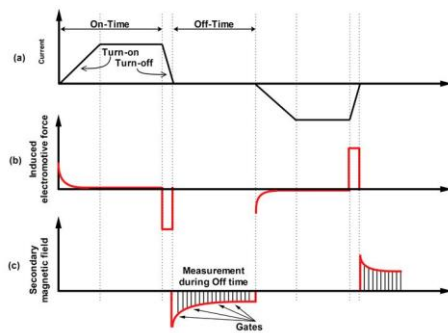


Fig. 5. Basic Nomenclature and Principles of the TEM.

Figure 5 defines the working and principles of TEM method.

- a) Current Signal injected in Transmitter Loop.
- b) EMF induced in surrounding Conductor.

- c) Secondary Magnetic Field produced in Receiver Coil.

3.2. TEM for Grounding Grid

Transmitter Coil is placed 50 cm above the ground and made up with pure copper (Copper selected from Built-In Materials of COMSOL) it is Torus shaped having major radius of 0.15 m and minor radius of 0.02 m all along 360 degrees the Transmitter coil is injected with 16A Current Pulse with wave form shown in the Figure 6 and the receiver coil is supposed to be the center point of the coil at which simulation data during OFF and ON time is extracted such as magnetic field intensities and EMF with time step of 10 μ s for 600 time samples during first 500 time steps the transmitter coil is ON and energized with 16A current pulse and for last 100 time samples transmitter coil is OFF and it is the vital data that is extracted in form of Text files for both Magnetic field intensities and EMF. The entire process is repeated for all the desired coordinates and the data is store in 8 different text files.

Magnetic field intensities of last 100 samples from 0.00501 sec to 0.006 sec are processed to calculate absolute average of all 100 values for each desired location.

EMF during OFF time of last 100 samples from 0.00501 sec to 0.006 sec are imported into MS Excel Spreadsheet and further these Excel sheets are called in MATLAB code that are used in the equations for further finding equivalent resistivity for all desired 8 locations are evaluated.

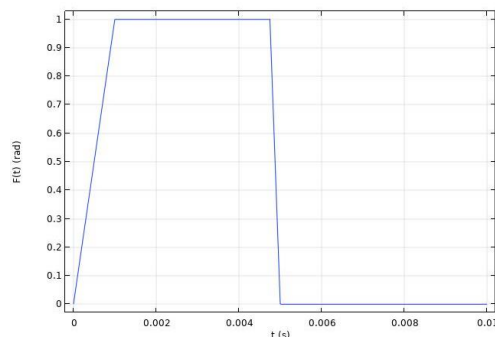


Fig. 6. Finalized Input Current Source Wave Form

3.3. Formulation of Apparent Resistivity

Magnetic field intensities are produced in all directions along all axis due to eddy currents the magnetic field intensity along z axis which is coming out of the earth surface can be easily found using.

$$Hz = \frac{I}{2a} \left[\frac{3}{\sqrt{\pi}u} e^{-u} + \left(1 - \frac{3}{2u^2}\right) \text{erf}(u) \right] \quad (1)$$

$u = \theta a$, “a” is the radius of the transmitter coil loop, erf(u) is error function of u variable.

By taking derivative with respect to u of Equation (1) we will have E(t)

$$\frac{dHz}{du} = E(t) = \frac{I}{\sigma a^3} \left[3 \text{erf}(u) - \frac{2}{\sqrt{\pi}} u(3 + 2u^2)e^{-u^2} \right] \quad (2)$$

Formula for calculating erf(u) is

$$\text{erf}(u) = \frac{2}{\sqrt{\pi}} \int_0^u e^{-t^2} dt \quad (3)$$

Error function gives us the value of probability for which if desired value is within the specified range.

u is the parameter of Transient Magnetic field and is expressed as following

$$u = \sqrt{\frac{\mu_o \sigma a^2}{4t}} = \theta a \quad (4)$$

Taking square of Equation (4) will give us following Equation.

$$u^2 = \frac{\mu_o \sigma a^2}{4t} \quad (5)$$

Rearranging the Equation (5) for the value of Conductivity (σ) we will get.

$$\sigma = \frac{4u^2 t}{\mu_o a^2} \quad (6)$$

Putting the value of conductivity in Equation (2).

$$E(t) = \frac{I}{\frac{4u^2 t}{\mu_o a^2} a^3} \left[3 \times \text{erf}(u) - \frac{2.0}{\sqrt{\pi}} \times u \times (3.0 + 2 \times u^2) \times e^{-u^2} \right] \quad (7)$$

$$E(t) = \frac{I \mu_o}{4u^2 t a} \left[3 \text{erf}(u) - \frac{2}{\sqrt{\pi}} u(3 + 2u^2)e^{-u^2} \right] \quad (8)$$

$$3 \text{erf}(u) - \frac{2}{\sqrt{\pi}} u(3 + 2u^2)e^{-u^2} - \frac{E(t)4u^2 t a}{I \mu_o} = 0 \quad (9)$$

Rewriting Equation (9) as function of u.

$$F(u) = 3 \text{erf}(u) - \frac{2}{\sqrt{\pi}} u(3 + 2u^2)e^{-u^2} - \frac{E(t)4u^2 t a}{I \mu_o} \quad (10)$$

As we know that conductivity and resistivity have inverse relation so

$$\rho = \frac{1}{\sigma} \quad (11)$$

Putting the value of conductivity (σ) in Equation (11) from Equation (6)

$$\rho(t) = \sqrt{\frac{\mu_o a^2}{4u^2 t}} \quad (12)$$

Parameter “u” can be obtained by optimizing Equation (10).

Apparent Resistivity at any sampling time t_i in terms of “u” can be expressed as

$$\rho(t_i) = \sqrt{\frac{\mu_o a^2}{4u^2 t_i}} \quad (13)$$

Equation for finding vertical depth (d) of induced eddy currents.

$$d = \frac{4}{\sqrt{\pi}} \sqrt{\frac{t \rho}{\mu}} \quad (14)$$

Equation for finding velocity (v) of induced eddy currents.

$$v = \frac{2}{\sqrt{\pi}} \sqrt{\frac{\rho}{t\mu}} \quad 15$$

Equation for finding Downward Velocity (v) between two consecutive samples

$$v = \frac{d_{i+1} - d_i}{t_{i+1} - t_i} \quad 16$$

Comparing Equation (15) and Equation (16)

$$\frac{d_{i+1} - d_i}{t_{i+1} - t_i} = \frac{2}{\sqrt{\pi}} \sqrt{\frac{\rho}{t\mu}} \quad 17$$

Taking square of the above Equation

$$\frac{(d_{i+1} - d_i)^2}{(t_{i+1} - t_i)^2} = \frac{4\rho}{\pi t\mu} \quad 18$$

Rearranging the above Equation (18)

$$\rho_r = \frac{(d_{i+1} - d_i)^2 (\pi t\mu)}{(t_{i+1} - t_i)^2 (4)} \quad 19$$

From Equation (14) depth can be rewritten for two consecutive time samples t_i and t_{i+1}

$$d_{i+1} - d_i = \frac{4}{\sqrt{\pi u}} (\sqrt{t_{i+1}\rho_{i+1}} - \sqrt{t_i\rho_i}) \quad 20$$

Taking square of the above Equation (20)

$$(d_{i+1} - d_i)^2 = \frac{16}{\pi\mu} (\sqrt{t_{i+1}\rho_{i+1}} - \sqrt{t_i\rho_i})^2 \quad 21$$

Putting Equation (20) in Equation (18)

$$\rho_r = \frac{\pi t\mu 16}{4\pi\mu} \cdot \frac{(\sqrt{t_{i+1}\rho_{i+1}} - \sqrt{t_i\rho_i})^2}{(\frac{1}{(t_{i+1}-t_i)})^2} \quad 22$$

Rearranging above Equation

$$\rho_r = 4t \cdot \left(\frac{\sqrt{t_{i+1}\rho_{i+1}} - \sqrt{t_i\rho_i}}{(t_{i+1} - t_i)} \right)^2 \quad 23$$

Here t is the average time of the consecutive samples can be expressed as

$$t = \frac{t_{i+1} + t_i}{2} \quad 24$$

Equivalent resistivity ρ_r can be calculated by using Equation (23) in Equation (22)

$$\rho_r = 4 \cdot \left(\frac{\sqrt{t_{i+1}\rho_{i+1}} - \sqrt{t_i\rho_i}}{(t_{i+1} - t_i)} \right)^2 \cdot \left(\frac{t_{i+1} + t_i}{2} \right) \quad 25$$

3.4. Mathematical Modelling

Function expressed in Equation (10) is the main function of the proposed research model.

Following 8 Inputs are used in the proposed functions to get desired outputs.

$e = 2.718$

$I =$ Transmitter Current = 16Amp

Vacuum Permeability = $4 \cdot \pi \cdot 10^{-7}$ H/m

$a =$ radius of transmitter loop = 0.15 m

$\sigma =$ conductivity of medium = $4.032 \cdot 10^6$ S/m

$t =$ sampling time = [0.00501:0.001:0.006] sec

Error Function = $erf(u) = \frac{2}{\sqrt{\pi}} \int_0^u e^{-u^2} dt$

Magnetic Permeability = $u = \sqrt{\frac{\mu_0 \sigma a^2}{4t}} = \theta a$

Following Outputs are obtained as end results.

Apparent Resistivity = $\rho(t) = \sqrt{\frac{\mu_0 a^2}{4u^2 t}}$

Apparent Resistivity is the resistivity of any material that can be derived from above mentioned formula using Vacuum / Magnetic Permeability, radius of transmitter Loop at any specific single time sample t .

Equivalent Resistivity = ρ_r

$$\rho_r = 4 \cdot \left(\frac{\sqrt{t_{i+1}\rho_{i+1}} - \sqrt{t_i\rho_i}}{(t_{i+1} - t_i)} \right)^2 \cdot \left(\frac{t_{i+1} + t_i}{2} \right)$$

Equivalent Resistivity is the basically the equivalence of two apparent resistivities of consecutive time samples such as off $\rho(t)$, $\rho(t + 1)$ and in the end average of these equivalent resistivities are calculated evaluated from all time samples.

4. Results and Discussions

4.1. Simulaton Model Designing

Both of the figures below Figure 7 and Figure 8 both are the designed models of

COMSOL Multiphysics the two Dimensional and 3-Dimensional View of the model the workspace dimensions are also mentioned top most layer is for Air and the bottom layer is for ground.

Ground Layer (Soil Material is selected from Minerals, Rocks and Soil section of Material Library in COMSOL) is square cube shaped 6 meter in length and 6 meter in width and the depth is 0.7 meters is set to be homogenous and its conductivity is set at 0.2 S/m and resistivity 5Ω.m.

Air Layer (Air Material Imported from Built-In Materials of COMSOL) is also solid square cube 6 meters in length and 6 meters in width and 0.3 meter in depth having set with the properties of air.

Grounding Grid Mesh is buried 0.5 meters below the Earth surface right in the middle having dimensions of 4x4 meter Grid consists of two 1.5x2 meter loops and two 3.5x2 meter loops connected together it is made up with Steel Alloy ASI 4340 imported from Built In Material List and having resistivity of $2.48 \times 10^{-7} \Omega.m$. The radius of the conductor is 10 cm.

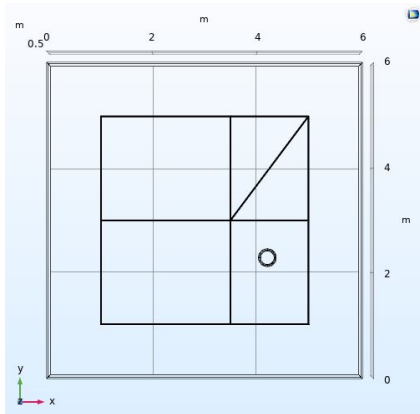


Fig. 7. COMSOL Multiphysics 2D Model of Unequally Spaced Mesh with Smaller Diagonal Branch for Simulation

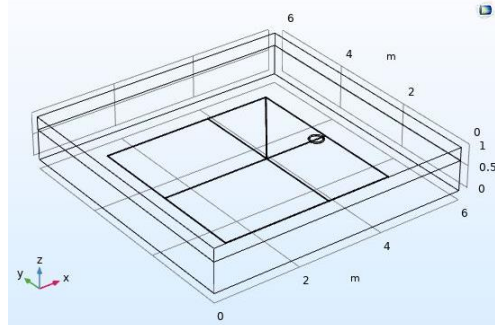


Fig. 8. COMSOL Multiphysics 3D Model of Unequally Spaced Mesh with Smaller Diagonal Branch for Simulation.

4.2. Calculations of Desired Coordinates

Here all coordinates are calculated for which simulations will take place in a circular path of 1m in radius and having center at the joining point of all four meshes which are equally spaced and the coordinates will be (3,3) from the Origin reference to model placement for simulation in COMSOL. So, by using the angles we can find out the x and y coordinates as following.

1. Coordinate C1 at θ_1 :

$$\theta_1 = 0^\circ$$

Radius of circle = $r = 1$ meter.

$$x_1 = r \cdot \cos \theta_1 = 1 \cdot \cos(0^\circ) = 1$$

$$y_1 = r \cdot \sin \theta_1 = 1 \cdot \sin(0^\circ) = 0$$

$$x_0 = 3, y_0 = 3,$$

$$(X_1, Y_1) = (x_0 + x_1, y_0 + y_1) \\ = (3 + 1, 3 + 0)$$

$$C_1 = (X_1, Y_1) = (4, 3)$$

2. Coordinate C2 at θ_2 :

$$\theta_2 = 45^\circ$$

Radius of circle = $r = 1$ meter.

$$x_2 = r \cdot \cos \theta_2 = 1 \cdot \cos(45^\circ) = 0.7071$$

$$y_2 = r \cdot \sin \theta_2 = 1 \cdot \sin(45^\circ) = 0.7071$$

$$x_0 = 3, y_0 = 3,$$

$$\begin{aligned} (X_2, Y_2) &= (x_0 + x_2, y_0 + y_2) \\ &= (3 + 0.7071, 3 \\ &\quad + 0.7071) \end{aligned}$$

$$C_2 = (X_2, Y_2) = (3.7071, 3.7071)$$

3. Coordinate C3 at θ_3 :

$$\theta_3 = 90^\circ$$

Radius of circle = $r = 1$ meter.

$$x_3 = r \cdot \cos \theta_3 = 1 \cdot \cos(90^\circ) = 0$$

$$y_3 = r \cdot \sin \theta_3 = 1 \cdot \sin(90^\circ) = 1$$

$$x_0 = 3, y_0 = 3$$

$$\begin{aligned} (X_3, Y_3) &= (x_0 + x_3, y_0 + y_3) \\ &= (3 + 0, 3 + 1) \end{aligned}$$

$$C_3 = (X_3, Y_3) = (3, 4)$$

4. Coordinate C4 at θ_4 :

$$\theta_4 = 135^\circ$$

Radius of circle = $r = 1$ meter.

$$x_4 = r \cdot \cos \theta_4 = 1 \cdot \cos(135^\circ) = -0.7071$$

$$y_4 = r \cdot \sin \theta_4 = 1 \cdot \sin(135^\circ) = 0.7071$$

$$x_0 = 3, y_0 = 3$$

$$\begin{aligned} (X_4, Y_4) &= (x_0 + x_4, y_0 + y_4) \\ &= (3 + (-0.7071), 3 \\ &\quad + 0.7071) \end{aligned}$$

$$C_4 = (X_4, Y_4) = (2.2929, 3.7071)$$

5. Coordinate C5 at θ_5 :

$$\theta_5 = 180^\circ$$

Radius of circle = $r = 1$ meter.

$$x_5 = r \cdot \cos \theta_5 = 1 \cdot \cos(180^\circ) = -1$$

$$y_5 = r \cdot \sin \theta_5 = 1 \cdot \sin(180^\circ) = 0$$

$$x_0 = 3, y_0 = 3$$

$$\begin{aligned} (X_5, Y_5) &= (x_0 + x_5, y_0 + y_5) \\ &= (3 + (-1), 3 + 0) \end{aligned}$$

$$C_5 = (X_5, Y_5) = (2, 3)$$

6. Coordinate C6 at θ_6 :

$$\theta_6 = 225^\circ$$

Radius of circle = $r = 1$ meter.

$$\begin{aligned} (X_6, Y_6) &= (x_0 + x_6, y_0 + y_6) \\ &= (3 + (-0.7071), 3 \\ &\quad + (-0.7071)) \end{aligned}$$

$$C_6 = (X_6, Y_6) = (2.2929, 2.2929)$$

7. Coordinate C7 at θ_7 :

$$\theta_7 = 270^\circ$$

Radius of circle = $r = 1$ meter.

$$x_7 = r \cdot \cos \theta_7 = 1 \cdot \cos(270^\circ) = 0$$

$$y_7 = r \cdot \sin \theta_7 = 1 \cdot \sin(270^\circ) = -1$$

$$x_0 = 3, y_0 = 3$$

$$\begin{aligned} (X_7, Y_7) &= (x_0 + x_7, y_0 + y_7) \\ &= (3 + (0), 3 + (-1)) \end{aligned}$$

$$C_7 = (X_7, Y_7) = (3, 2)$$

8. Coordinate C8 at θ_8 :

$$\theta_8 = 315^\circ$$

Radius of circle = $r = 1$ meter.

$$x_8 = r \cdot \cos \theta_8 = 1 \cdot \cos(315^\circ) = 0.7071$$

$$y_8 = r \cdot \sin \theta_8 = 1 \cdot \sin(315^\circ) = -0.7071$$

$$x_0 = 3, y_0 = 3$$

$$\begin{aligned} (X_8, Y_8) &= (x_0 + x_8, y_0 + y_8) \\ &= (3 + 0.7071, 3 \\ &\quad + (-0.7071)) \end{aligned}$$

$$C_8 = (X_8, Y_8) = (3.7071, 2.2929)$$

4.3. Selected Grounding Grid Models Layouts

Basic Layout of all the Grounding Grids is same with some minor changes such as the position of diagonal branches and the size of these diagonal branches and the quantity of these branches.

All the proposed models are mentioned below each of them mentioned with their changes

- a) Unequally spaced grounding grid with smaller diagonal branch.

- b) Unequally spaced grounding grid with larger diagonal branch.
- c) Unequally spaced grounding grid with both smaller and larger diagonal branches.

In the Figure 9 only one diagonal branch is present denoted by conductor S13 meeting the nodes 5 and 9 in the first mesh of the grid which is smaller in size located between the nodes 5,6,9 and 8.

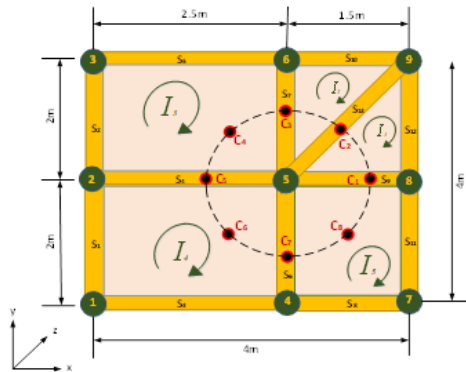


Fig. 9. Grounding Grid Layout of Unequally Spaced Grounding Grid with Diagonal Branch in the Smaller Mesh.

In the Figure 10 only one diagonal branch is present denoted by conductor S13 meeting the nodes 5 and 1 in the third mesh of the grid which is larger in size located between the nodes 1,2,5 and 4.

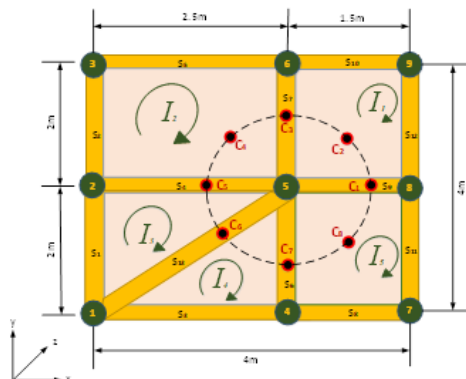


Fig. 10. Grounding Grid Layout of

Unequally Spaced Grounding Grid with Diagonal Branch in the Larger Mesh.

In this model Grid has both diagonals mentioned above both smaller and larger in same meshes 1st and 3rd.

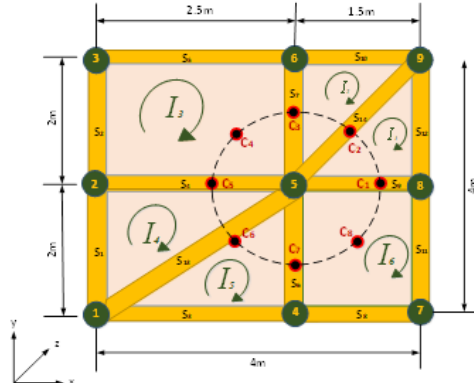


Fig. 11. Grounding Grid Layout of Unequally Spaced Grounding Grid with 2 Diagonal Branches in both Smaller and Larger Mesh.

4.4. Discussion on Results of All The Proposed Models

Comparative Graphs of all the results of the proposed models are given below for equivalent resistivity and magnetic field intensity.

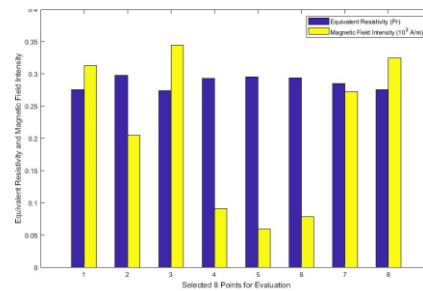


Fig. 12. Equivalent Resistivity and Magnetic Field Intensities Comparative Plot at all Measuring 8 Coordinates of Unequally Spaced Grounding Grid with Diagonal Branch in Smaller Mesh.

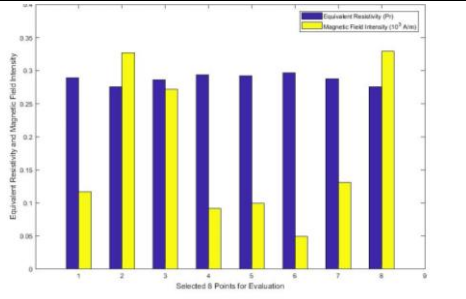


Fig. 13. Equivalent Resistivity and Magnetic Field Intensities Comparative Plot at all Measuring 8 Coordinates of Unequally Spaced Grounding Grid with Diagonal Branch in Larger Mesh.

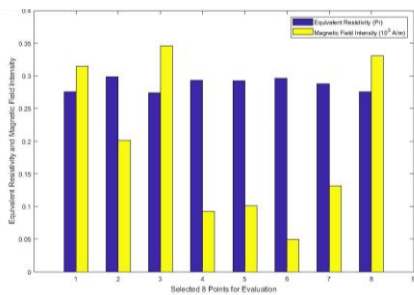


Fig. 14. Equivalent Resistivity and Magnetic Field Intensities Comparative Plot at all Measuring 8 Coordinates of Unequally Spaced Grounding Grid with 2 Diagonal Branches in both Smaller and Larger Mesh.

Numerical figures derived from the above-mentioned graphs in Figure 12, Figure 13 and Figure 14 of equivalent resistivities and magnetic field intensities which are shown in table format below it is much easier for interpretation and comparative analysis.

This space is intentionally left blank to adjust tables on other column.

Table 1: Average Equivalent Resistivities at all the Specified Coordinates of the Experimented Models.

Measuring Coordinate	Average Equivalent Resistivity ($\Omega\text{-m}$)		
	<i>Unequally spaced Mesh with Smaller Diagonal</i>	<i>Unequally spaced Mesh with Larger Diagonal</i>	<i>Unequally spaced Mesh with both Smaller and Larger Diagonal</i>
C ₁	0.2758	0.2889	0.2758
C ₂	0.2982	0.2752	0.2982
C ₃	0.2736	0.2856	0.2736
C ₄	0.2933	0.2933	0.2933
C ₅	0.2955	0.2922	0.2922
C ₆	0.2944	0.2965	0.2965
C ₇	0.2851	0.2878	0.2878
C ₈	0.2752	0.2752	0.2752

Table 2: Average Magnetic Field Intensities at all the specified coordinates of the experimented models.

Measuring Coordinate	Average Magnetic Field Intensity (A/m)		
	<i>Unequally spaced Mesh with Smaller Diagonal</i>	<i>Unequally spaced Mesh with Larger Diagonal</i>	<i>Unequally spaced Mesh with both Smaller and Larger Diagonal</i>
C ₁	313.16	116.05	313.68
C ₂	205.06	326.81	200.92
C ₃	344.96	271.71	345.69
C ₄	90.3	91.02	92.43
C ₅	59.3	98.97	101.1
C ₆	78.38	48.77	48.77
C ₇	272.11	130.91	131.47
C ₈	325.17	329.16	330.47

Coordinates C₄ and C₈ are identical in all three models so as a result they have same values for Equivalent resistivity and Magnetic field intensity for all three proposed models because these lies in the middle of the

meshes where there are no diagonal branches in the middle of 2nd and 4th mesh here overall resistivity and magnetic field intensity is not affected by the diagonal branches in the neighboring meshes.

C₄ has low magnetic field intensity due to larger size mesh and low current flows so the equivalent resistivity is higher and C₈ has higher magnetic field intensities due to smaller mesh and higher current flow so the equivalent resistivity will decrease.

1st model in Figure 9 and the 3rd model in Figure 11 both have identical 1st mesh here at C₁ two currents flows I₁ and I₅ in case of first model both current are flowing through different sized meshes so both currents are not same and opposing each other so as a result significant net current flows which increases the MFI relatively to 2nd highest overall and minimize the equivalent resistivity.

At Coordinate C₁ Currents I₁ and I₅ in 2nd model (Figure 10) are equal and opposite in direction due to non-presence of diagonal element so very low current flows and MFI is relatively smaller and equivalent resistivity is higher.

Similarly, at Coordinate C₂ currents I₁ and I₂ for 1st and 3rd model are equal yet opposite in direction and nullify each other as a result very least current flows so we get higher equivalent resistivity and relatively lower MFI.

C₂ Coordinate in 2nd Model Figure 10 is in the middle of the smaller mesh with strong magnetic field and produces large eddy currents so we get higher magnetic field intensity and low equivalent resistivity.

Coordinate C₃ has same results for 1st and 3rd model because of same configuration currents I₂ and I₃ flowing through C₃ are unequal and opposite due to presence of diagonal branch in smaller mesh and the net current is relatively higher because current flowing I₂ is higher than the current I₃ lower so some significant current flows as a result equivalent resistivity is lower and MFI is the highest.

Coordinate C₃ in 2nd model Figure 10 will have moderate MFI and Moderate equivalent resistivity coz of moderate current flowing through it I₂ with lesser value and I₁ with higher value opposing each other and net current is moderate.

From Coordinate C₅ to so on the 2nd model Figure 10 is same as the 3rd model Figure 11 so the output result of both models are approximately same, at C₅ in 1st model Figure 10 there is no larger diagonal so it lies in between the larger meshes which are already flowing lesser currents I₃ and I₄ opposite to each other so nullifies each other and net current is the least of all as a result equivalent resistance is highest of all and the MFI is least of all the values of 1st Model Figure 9.

C₅ in 2nd and 3rd Model has a neighboring larger diagonal branch due to which in case of 2nd Model Figure 10 two currents are flowing from C₅ I₂ and I₃, I₃>I₂ so some net current flows as a result of the opposition so equivalent resistance is relatively smaller and MFI is relatively larger than C₄ but still less than C₇.

C₆ coordinate in case of 1st model Figure 9 lies in almost at the middle of mesh no 3 the weak magnetic fields are produced due to the larger mesh size so lesser eddy currents are induced as a result larger value of equivalent resistivity but not the least and weaker MFI but still larger than C₅.

C₆ for 2nd and 3rd model are same and have almost same values as it lies almost on top of the large diagonal branch where in case of 2nd Model I₃ and I₄ flowing opposite to each other and with exactly same values which are lesser due to larger diagonal branch size and net current is the least of all the others even considering all other models too so the equivalent resistivity is the highest of all the models and Magnetic Field intensity is the least of all the other models.

C₇ coordinate in case of 1st model Figure 9 correlates to C₃ in 2nd Model Figure 10 and have almost same values of equivalent

resistivity and magnetic field intensities describer earlier.

C₇ coordinate in 2nd model Figure 10 and 3rd model Figure 11 has same results due to same configuration in case of 2nd model Figure 10 currents I₄ and I₅ are flowing from C₇ both of these currents are not similar and opposite to each other due to which some net current flows which is lesser than the current of C₇ in model no 1 and has a bit lesser magnetic field intensity and a bit higher equivalent resistivity than C₇ in model no 1

5. Conclusion and Future Scope

Starting from the scratch the physical position of a single grounding conductor leads onto finding the complete oriented angle of the grounding grid.

Magnetic field intensities in the middle of smaller loops are stronger than the middle of bigger loops and the equivalent resistivity in the middle of the smaller loops are greater than the equivalent resistivity at the middle of the bigger loops.

Diagonal Elements at the middle of the Loops increases the Equivalent resistance and decreases the Magnetic field intensity.

Conductor shared by the bigger loops have the least value of Magnetic field intensity and highest value Equivalent resistivity.

Diagonal Branches and unequal sizes of loops results in unbalanced and unequal flowing currents.

Magnetic Field Intensity on the diagonal branch of smaller loop is greater than the diagonal branch of larger loop.

There is still scope in finding the configuration of grounding grid using Transient Electromagnetic Method as it will be next feasible step taken in fault diagnosis of grounding grid after orientation detection.

AUTHOR CONTRIBUTION

Usman Zia Saleem: Conceptualization, Methodology, Software, Validation, Investigation. Safdar Raza: Supervision, Project Administration, Investigation.

Inzamam Ul Haq: Resources, Data Curation, Formal analysis. Muhammad Bilal Ashraf: Writing - Review & Editing, Writing - Original Draft.

DATA AVAILABILITY STATEMENT

The datasets generated during and analyzed during the current study are available from the corresponding author on reasonable request.

CONFLICT OF INTEREST

Authors of this paper declare no conflict of interest.

FUNDING

This paper is composed from research that was not funded by any organization or institution.

REFERENCES

- [1] IEEE Guide for Safety in AC Substation Grounding," IEEE Std 80-2000, pp. 1-192, 2000, doi: 10.1109/IEEESTD.2000.91902.
- [2] IEEE Std 80-2013 (Revision of IEEE Std 80-2000/ Incorporates IEEE Std 80-2013/Cor 1-2015) - Redline. IEEE, 2015.
- [3] B. Zhang, J. Wu, J. He, and R. Zeng, "Analysis of transient performance of grounding system considering soil ionization by time domain method," IEEE Transactions on Magnetics, vol. 49, no. 5, pp. 1837-1840, 2013.
- [4] N. Eghtedarpour, M. Karimi, and M. Tavakoli, "Analyzing the effect of substation grounding system on distance relays operation: a documented case," in 2019 International Power System Conference (PSC), 2019: IEEE, pp. 275-279.
- [5] S. Huang, Z. Fu, Q. Wang, X. Zhu, and S. Qin, "Service life estimation for the small-and medium-sized earth grounding grids," IEEE Transactions on Industry Applications, vol. 51, no. 6, pp. 5442-5451, 2015.
- [6] L. M. Popović, "Reduction of the fault current passing through the grounding system of an HV substation supplied by cable line," International Journal of Electrical Power & Energy Systems, vol. 99, pp. 493-499, 2018.
- [7] E.-S. M. El-Refaie, S. E. Elmasry, M. Abd Elrahman, and M. H. Abdo, "Achievement of the best design for unequally spaced

- grounding grids," *Ain Shams Engineering Journal*, vol. 6, no. 1, pp. 171-179, 2015.
- [8] M. Mitolo, P. E. Sutherland, and R. Natarajan, "Effects of high fault currents on ground grid design," *IEEE Transactions on Industry Applications*, vol. 46, no. 3, pp. 1118-1124, 2010.
- [9] M. Lorentzou, N. Hatziargyriou, and B. Papadias, "Time domain analysis of grounding electrodes impulse response," *IEEE Transactions on power delivery*, vol. 18, no. 2, pp. 517-524, 2003.
- [10] Y. Liu, N. Theethayi, and R. Thottappillil, "An engineering model for transient analysis of grounding system under lightning strikes: Nonuniform transmission-line approach," *IEEE Transactions on Power Delivery*, vol. 20, no. 2, pp. 722-730, 2005.
- [11] R. Lucić, I. Jurić-Grgić, and Z. Balaž, "Grounding grid transient analysis using the improved transmission line model based on the finite element method," *International Transactions on Electrical Energy Systems*, vol. 23, no. 2, pp. 282-289, 2013.
- [12] F. Xu, C. Liu, W. Hong, and K. Wu, "Fast and accurate transient analysis of buried wires and its applications," *IEEE Transactions on Electromagnetic Compatibility*, vol. 56, no. 1, pp. 188-199, 2013.
- [13] A. Jardines, J. Guardado, J. Torres, J. Chavez, and M. Hernandez, "A multiconductor transmission line model for grounding grids," *International Journal of Electrical Power & Energy Systems*, vol. 60, pp. 24-33, 2014.
- [14] M. Ramamoorthy, M. B. Narayanan, S. Parameswaran, and D. Mukhedkar, "Transient performance of grounding grids," *IEEE Transactions on Power Delivery*, vol. 4, no. 4, pp. 2053-2059, 1989.
- [15] B. Zhang et al., "Numerical analysis of transient performance of grounding systems considering soil ionization by coupling moment method with circuit theory," *IEEE Transactions on Magnetics*, vol. 41, no. 5, pp. 1440-1443, 2005.
- [16] L. D. Grcev and M. Heimbach, "Frequency dependent and transient characteristics of substation grounding systems," *IEEE Transactions on Power Delivery*, vol. 12, no. 1, pp. 172-178, 1997.
- [17] V. Dorić, D. Poljak, and V. Roje, "Transient analysis of the grounding electrode based on the wire antenna theory," *Engineering analysis with boundary elements*, vol. 28, no. 7, pp. 801-807, 2004.
- [18] D. Poljak and V. Doric, "Wire antenna model for transient analysis of simple grounding systems, Part I: The vertical grounding electrode," *Progress in electromagnetics research*, vol. 64, pp. 149-166, 2006.
- [19] D. Poljak and V. Doric, "Wire antenna model for transient analysis of simple grounding systems, Part II: The horizontal grounding electrode," *Progress in electromagnetics research*, vol. 64, pp. 167-189, 2006.
- [20] D. Cavka, B. Harrat, D. Poljak, B. Nekhoul, K. Kerroum, and K. E. K. Drissi, "Wire antenna versus modified transmission line approach to the transient analysis of grounding grid," *Engineering analysis with boundary elements*, vol. 35, no. 10, pp. 1101-1108, 2011.
- [21] S. Šesnić and D. Poljak, "Antenna model of the horizontal grounding electrode for transient impedance calculation: Analytical versus boundary element method," *Engineering Analysis with Boundary Elements*, vol. 37, no. 6, pp. 909-913, 2013.
- [22] B. Nekhoul et al., "An efficient transient analysis of realistic grounding systems: transmission line versus antenna theory approach," *Engineering Analysis with Boundary Elements*, vol. 48, pp. 14-23, 2014.
- [23] A. Qamar, I. Ul Haq, M. Alhaisoni, and N. N. Qadri, "Detecting Grounding Grid Orientation: Transient Electromagnetic Approach," *Applied Sciences*, vol. 9, no. 24, p. 5270, 2019.
- [24] Y. Liu, L. Xiao, and J. Tian, "Optimized corrosion diagnosis of large-scale grounding grid," in *IEEE PES General Meeting, 2010: IEEE*, pp. 1-6.
- [25] X. Zhu, L. Cao, J. Yao, L. Yang, and D. Zhao, "Research on ground grid diagnosis with topological decomposition and node voltage method," in *2012 Spring Congress on Engineering and Technology, 2012: IEEE*, pp. 1-4.
- [26] L. J. Li, M. F. Peng, and K. X. Zhao, "Fault diagnosis for grounding grids based on genetic algorithm and support vector machine," in *Advanced Materials Research, 2013, vol. 787: Trans Tech Publ*, pp. 909-913.
- [27] D. Wang and B. He, "Practicality analysis for fault diagnosis of medium-scale grounding grid," in *2016 IEEE International Conference on High Voltage Engineering and Application (ICHVE), 2016: IEEE*, pp. 1-4.
- [28] F. Yang et al., "A cycle voltage measurement method and application in grounding grids fault location," *Energies*, vol. 10, no. 11, p. 1929, 2017.
- [29] X.-L. Zhang, X.-H. Zhao, Y.-G. Wang, and N. Mo, "Development of an electrochemical in situ detection sensor for grounding grid corrosion," *Corrosion*, vol. 66, no. 7, pp. 076001-076001-7, 2010.

- [30] Y. Liu, X. Cui, and Z. Zhao, "A magnetic detecting and evaluation method of substation's grounding grids with break and corrosion," *Frontiers of Electrical and Electronic Engineering in China*, vol. 5, no. 4, pp. 501-504, 2010.
- [31] C. Yu, Z. Fu, X. Hou, H.-M. Tai, and X. Su, "Break-point diagnosis of grounding grids using transient electromagnetic apparent resistivity imaging," *IEEE Transactions on Power Delivery*, vol. 30, no. 6, pp. 2485-2491, 2015.
- [32] C. Yu, Z. Fu, Q. Wang, H.-M. Tai, and S. Qin, "A novel method for fault diagnosis of grounding grids," *IEEE Transactions on Industry Applications*, vol. 51, no. 6, pp. 5182-5188, 2015.
- [33] L. Xiang and X. Cui, "Detecting method of conductors and mesh structure of substation's grounding grids," *Trans. China Electrotech. Soc.*, vol. 28, no. 5, pp. 167-173, 2013.
- [34] L. Chunli, H. Wei, Y. Degui, Y. Fan, K. Xiaokuo, and W. Xiaoyu, "Topological measurement and characterization of substation grounding grids based on derivative method," *International Journal of Electrical Power & Energy Systems*, vol. 63, pp. 158-164, 2014.
- [35] A. Qamar, F. Yang, W. He, A. Jadoon, M. Z. Khan, and N. Xu, "Topology Measurement of Substation's Grounding Grid by Using Electromagnetic and Derivative Method," *Progress In Electromagnetics Research*, vol. 67, pp. 71-90, 2016.
- [36] C. Yu, Z. Fu, G. Wu, L. Zhou, X. Zhu, and M. Bao, "Configuration detection of substation grounding grid using transient electromagnetic method," *IEEE Transactions on Industrial Electronics*, vol. 64, no. 8, pp. 6475-6483, 2017.
- [37] A. Qamar, F. Yang, N. Xu, and S. A. Shah, "Solution to the inverse problem regarding the location of substation's grounding grid by using the derivative method," *International Journal of Applied Electromagnetics and Mechanics*, vol. 56, no. 4, pp. 549-558, 2018.
- [38] A. K. Mohamed, M. A. Meju, and S. L. Fontes, "Deep structure of the northeastern margin of the Parnaiba Basin, Brazil, from magnetotelluric imaging," *Geophysical Prospecting*, vol. 50, no. 6, pp. 589-602, 2002.
- [39] G. Xue, Y. Yan, X. Li, and Q. Di, "Transient electromagnetic S-inversion in tunnel prediction," *Geophysical Research Letters*, vol. 34, no. 18, 2007.
- [40] M. Metwaly, G. El-Qady, U. Massoud, A. El-Kenawy, J. Matsushima, and N. Al-Arifi, "Integrated geoelectrical survey for groundwater and shallow subsurface evaluation: case study at Siliyin spring, El-Fayoum, Egypt," *International Journal of Earth Sciences*, vol. 99, no. 6, pp. 1427-1436, 2010.
- [41] H. Tang, H. Yang, G. Lu, S. Chen, J. Yue, and Z. Zhu, "Small multi-turn coils based on transient electromagnetic method for coal mine detection," *Journal of Applied Geophysics*, vol. 169, pp. 165-173, 2019.
- [42] P. Wang, M. Li, W. Yao, C. Su, Y. Wang, and Q. Wang, "Detection of abandoned water-filled mine tunnels using the downhole transient electromagnetic method," *Exploration Geophysics*, pp. 1-16, 2020.
- [43] G. Xue, W. Chen, S. Yan, N. Zhou, and D. Qingyun, "Device and method for ground source transient electromagnetic near-field detection and related device," ed: Google Patents, 2020.
- [44] Z. Ye, C. Zhang, Y. Ye, and W. Zhu, "Application of transient electromagnetic radar in quality evaluation of tunnel composite lining," *Construction and Building Materials*, vol. 240, p. 117958, 2020.